

RESULTS OF A LOW-SPEED WIND TUNNEL TEST OF THE MDC 2.2M
SUPERSONIC CRUISE AIRCRAFT CONFIGURATION*

R.L. Roensch, J.E. Felix, and H.R. Welge
Douglas Aircraft Company
McDonnell Douglas Corporation

L.P. Yip and L.P. Parlett
Langley Research Center

SUMMARY

Results of a low-speed test conducted in the Full Scale Tunnel at NASA Langley using an advanced supersonic cruise vehicle configuration are presented. These tests were conducted using a ten-percent scale model of a configuration developed by McDonnell Douglas that had demonstrated high aerodynamic performance at Mach 2.2 during a previous test program. The low-speed model has leading- and trailing-edge flaps designed to improve low-speed lift-to-drag ratios at high lift and includes devices for longitudinal and lateral/directional control.

The results obtained during the low-speed test program have shown that full-span leading-edge flaps are required for maximum performance. The amount of deflection of the leading-edge flap must increase with C_L to obtain the maximum benefit. Over eighty percent of full leading-edge suction was obtained up to lift-off C_L 's of 0.65.

A mild pitch-up occurred at about 6° angle of attack with and without the leading-edge flap deflected. The pitch-up is controllable with the horizontal tail. Spoilers were found to be preferable to spoiler/deflectors at low speeds. The vertical tail maintained effectiveness up to the highest angle of attack tested but the tail-on directional stability deteriorated at high angles of attack. Lateral control was adequate for landing at 72 m/sec (140 knots) in a 15.4 m/sec (30 knot) crosswind.

It is recommended that in the future the drag-due-to-lift characteristics be validated at higher Reynolds numbers. Also fuselage strakes to improve directional stability and leading-edge slats to improve low speed lift-to-drag ratios should be considered for future testing. The impact of recent wing modifications developed for high-speed drag improvement need to be assessed at low speed.

INTRODUCTION

McDonnell Douglas (MDC) and NASA have been working jointly on the development of technology for Advanced Supersonic Cruise vehicles over the past several years. As part of this development a 1.5-percent scale high-speed wind tunnel test program was run at the NASA Ames Research Center in 1975 (ref. 1) which demonstrated that, for the configuration designed by MDC, high aerodynamic performance levels were achieved. To supplement these high-speed data, a

*This work was performed under NASA Contract NAS1-14621

ten-percent scale model of the same configuration for test at low speed was constructed by NASA using inputs from MDC for the geometry of the high-lift and low-speed control devices. These tests would measure force data and surface pressures as in the previous high speed tests, and would give a complete data base on one configuration for Mach numbers from near zero (0.09) to $M = 2.4$.

This low speed ten-percent scale model was tested by NASA in the Full Scale Tunnel at the Langley Research Center. This paper presents a summary of the current status of the analysis of these test results.

SYMBOLS

AR	wing aspect ratio
C_D	drag coefficient
C_{D_0}	minimum clean (no leading- or trailing-edge deflection) configuration drag coefficient
C_L	lift coefficient
C_M	pitching moment coefficient about the quarter chord
ΔC_{ℓ}	incremental rolling moment coefficient
C_{N_β}	variation of yawing moment coefficient with sideslip angle
ΔC_{N_v}	change in yawing moment coefficient due to vertical tail
C_p	pressure coefficient
i_H	incidence of horizontal tail relative to fuselage reference system, degrees
L/D	lift-to-drag ratio
M_0	free stream Mach number
S	leading edge suction parameter
α or alpha	fuselage reference system angle of attack, degrees
β	angle of sideslip, degrees
δ_a	aileron deflection angle, degrees
δ_F	trailing edge flap deflection angle, degrees
δ_{LE}	leading edge flap deflection angle normal to the leading edge, degrees
η	percent wing semispan

DESCRIPTION OF THE MODEL

The dimensional characteristics of the ten-percent scale model are shown in figure 1. A photograph of the model mounted in the Langley Full Scale Tunnel is shown in figure 2. The model was constructed of fiberglass over an aluminum frame and was essentially rigid for this test.

The wing consisted of an arrow planform with an inboard leading-edge sweep angle of 71 degrees and an outboard sweep angle of 57 degrees with a leading edge break at 63 percent of the semi-span. The wing was constructed with four segments of leading-edge flaps inboard of the leading-edge break and two segments outboard of the leading-edge break. The wing had an inboard and outboard single-slot trailing-edge flap system. The model had the inboard and mid slotted spoiler/deflectors installed on the right hand wing, and the outboard inverted spoiler/deflector installed on the left hand wing. They were only tested asymmetrically for their effect on roll control. The model was instrumented with 270 pressure orifices distributed among five spanwise rows over the wing. The pressures were obtained using scanivalve transducers. A schematic drawing of the leading- and trailing-edge flaps, and the spoiler/deflector system, and the spanwise location of the pressure rows are shown on figure 3 and the variable geometry features of the model are illustrated in figure 4. Indicated are the available deflections of the leading-edge flaps (measured normal to the leading edge) and the letter code designation of the combinations of deflections for which data are presented in this paper.

TESTS AND CORRECTIONS

Tests were made in the Langley Full Scale Tunnel at a freestream dynamic pressure of $q = 575 \text{ Pa}$ (12 psf or $M_0 = 0.09$). The tests were conducted over an angle of attack range from about -6 degrees to 23 degrees and over a sideslip range from -15 degrees to 20 degrees. The Reynolds number based on the mean aerodynamic chord of 1.975 m (6.48 ft) was 4.18×10^6 .

The model was tested upright and inverted with a single dummy strut, (figure 5) to evaluate the flow angularity and strut tares which were applied to the data. Buoyancy corrections were computed and applied to the data. Blockage corrections were applied based on tunnel surveys from previous tests of similar size models. Wall corrections were not applied based on previous tests (ref. 2 and 3).

RESULTS

WING-BODY LONGITUDINAL FORCE DATA

Prior to obtaining the basic aerodynamic characteristics of the configuration, an initial study was conducted to determine the best leading-edge flap deflection. The effect of deflecting the leading-edge flaps over only part of the span is shown on figure 6. Selectively eliminating leading-edge deflections over the inner, middle or outer wing panel produce higher drags at lift coefficients greater than 0.4 than full-span leading-edge deflections. No advantages were found in the lift or pitching moment to warrant part span leading-edge flap deflection.

The aerodynamic characteristics for increasing amounts of full-span leading-edge flap deflection are shown in figures 7 through 12 for zero and 30 degrees of trailing-edge flaps. For the case of zero flaps, the lift-curve break at about 5 degrees ($C_L \approx 0.2$) indicates the condition where a leading-edge vortex begins to form. The smallest angle of deflection for the leading-edge flaps tested results in a nearly linear lift curve which implies elimination of the leading-edge vortex. Significant reductions in the drag are also obtained for this deflection. The inception of the non-linear nose-up pitching-moment break at about six degrees angle of attack is not affected by deflecting the leading-edge flaps, although the magnitude of the pitch-up is reduced. Further deflection of the leading-edge flaps has little effect on the drag and lift with a small effect on pitching moments.

With the trailing-edge flaps deflected, the smallest leading-edge flap deflection also eliminates the break in the lift curve and leading-edge vortex. In this case, because the deflection of trailing-edge flaps cause more leading-edge load for a given angle of attack, the breakdown in the lift curve occurs at two degrees angle of attack. However, because of the lift the flap produces, the break in the lift curve occurs at a C_L of 0.3 instead of 0.2 with the flaps up. With the trailing-edge flaps down there is less effect of the leading-edge flap deflection on drag or pitching moments than with the flaps up.

Based on the above results, the longitudinal, lateral-directional and tail effectiveness characteristics were conducted with leading-edge flap deflection R.

The lift and pitching moment characteristics for the clean configuration (leading- and trailing-edge flaps retracted) are compared in figures 13 and 14 to the Douglas 3-D Neumann Potential Flow Program (ref. 4) results run at $M_o = 0$ and to previous data obtained on a 1.5-percent scale high-speed model (ref. 1) at $M_o = 0.5$. Adjustments to the data have not been made to correct for the Mach number difference between the two tests. The characteristics of the ten-percent low-speed model lift and pitching moment results agree very well with the previous test results except for a one degree shift in the angle of attack for zero lift. The 3-D Neumann lift-curve slope agrees with the data prior to the inception of vortex lift but the angle of attack for zero lift is shifted by about two degrees.

The drag results are compared to full and zero leading-edge suction calculations in addition to the 3-D Neumann results (which have been shifted to agree with the test data at minimum drag) and the previous 1.5-percent scale data in figure 15. The data show that 60 to 40 percent of full leading edge suction is obtained for a C_L range of 0.2 to 0.8. The Neumann results are close to full leading-edge suction as expected and do not agree well with the data. The previous 1.5 percent scale results were obtained at about the same Reynolds number based on the mean aerodynamic chord (4×10^6) and the agreement with the low speed data is within acceptable limits.

The results with deflected leading-edge flaps and zero deflection of the trailing-edge flaps are shown in figures 16 through 18. These results are also compared to the Neumann and full and zero leading-edge suction. Similar

comments as before apply to the lift and moment comparison with the Neumann results. Drag results indicate that leading edge suction is nearly 100 percent at low C_L 's diminishing to about 40 percent as the C_L is increased.

Drag results with the leading- and trailing-edge flaps deflected are shown on figure 19. The Neumann results are not yet available for this case. About 80 percent of full leading-edge suction is obtained over a wide range of C_L 's.

A summary of the leading-edge suction results are shown on figure 20. Seventy- to eighty-percent full leading-edge suction is obtained with the trailing-edge flaps deflected 30 degrees with or without the leading-edge flaps deflected. For the optimum trailing-edge flap setting as a function of C_L , leading-edge suction over 80 percent is achieved up to the lift-off C_L of 0.65. These data also indicate that higher leading-edge flap deflections are required as the C_L is increased. Recent results obtained by Coe (ref. 5) for a wing with higher sweep and lower aspect ratio (SCAT 15) are slightly below the current results. Recent additional data by Coe (ref. 6) have shown that further improvements are possible.

The untrimmed lift-to-drag (L/D) ratio results are shown on figure 21 for several leading- and trailing-edge deflections. These results have been corrected to the full scale Reynolds number. L/D's slightly over ten were obtained in the C_L range for climb-out ($C_L \approx 0.3$) dropping off to about 5.5 at the lift-off C_L 's near 0.65. Also shown are the previous 1.5 percent scale high speed model test data, estimates made prior to the test, and recent test data from Coe (ref. 5). The 1.5 percent scale model results show slightly higher L/D's than the low speed model at C_L 's in the 0.2 range with the agreement improving as the C_L is increased. The relatively small drag differences shown earlier (fig. 15) produce this discrepancy. The pre-test estimates, which are indicative of the levels used to calculate the low-speed performance of the aircraft, were made without the benefit of any data-base on leading-edge devices of this type and are higher than the measured values. Recent data from Coe (ref. 5), had it been available, would have been valuable in improving these estimates. The configuration L/D obtained by Coe agrees with the current results if adjusted for aspect ratio.

WING-BODY PRESSURE DATA

The experimental upper surface pressure distributions for the clean configuration at three angles of attack are shown on figure 22. The increase of the pressure peak near the leading edge and the shape of the pressure distribution illustrates the formation of the leading-edge vortex. The aft movement of the vortex is evident at the 64 percent semi-span station as the negative pressures move progressively aft as the angle of attack is increased. At 13 degrees angle of attack, there appears to be a second vortex present as illustrated by the second negative pressure peak between 50 and 70 percent chord at the 49 percent semi-span station.

The pressure peak on the inner panel with its rounded leading edge continues to increase with angle of attack. In contrast, the constant C_p level of 0.5 to 0.75 at the leading edge of the outer panel at all angles suggests that,

because of the sharp leading edge, the outer panel vortex forms at very low angles of attack.

The experimental pressure distributions are compared to the 3-D Neumann results at an angle of attack of one degree ($C_L \approx 0.05$) prior to the inception of vortex lift on figure 23. The agreement is reasonable on the rounded leading edge inner panel but agreement deteriorates on the sharp leading edge outer panels. This confirms the fact that the sharp outer panel leading edge cannot carry the loads required to produce a potential flow, i.e., no vortex, at essentially any C_L .

Comparisons with and without the leading-edge flaps deflected are shown in figure 24 at a higher C_L of 0.35 ($\alpha = 9^\circ$) after the inception of vortex lift. The general character of the experimental pressure distribution is represented by the theory with the leading-edge flaps deflected but there is some disagreement in level. The data at 49-percent semi-span station illustrates the effect of the leading-edge vortex on the potential pressures without leading-edge flap deflection.

HORIZONTAL TAIL EFFECTIVENESS

Effectiveness of the horizontal tail for the landing configuration is shown in figure 25. At low angles of attack, (below 5 deg) the tail contributes to the longitudinal stability of the airplane, shifting the neutral point aft by 5% of the MAC. At angles of attack above 5 degrees, the aircraft pitches up and the tail-off neutral point shifts forward. The tail contribution to longitudinal stability is close to zero at angles of attack above 5 degrees. Tail effectiveness for pitch control is maintained to the highest angles tested. The reduced stability contribution without loss of effectiveness is attributed to a strong downwash gradient at the location of the horizontal tail.

DIRECTIONAL STABILITY AND VERTICAL TAIL EFFECTIVENESS

Directional stability of the aircraft tail-on and tail-off is illustrated in figure 26 and the contribution of the vertical tail to directional stability is shown in figure 27. Directional stability without leading- or trailing-edge flaps deflected is maintained at a reasonably constant level at angles of attack up to about $12\frac{1}{2}$ degrees (fig. 26) and is gradually reduced at higher angles until neutral stability is reached at about 20 degrees. The reduced stability at high angles of attack is due to a combination of reduced tail-off stability which begins at $12\frac{1}{2}$ degrees and reduced tail effectiveness (fig. 27) which begins at about 15 degrees.

In the landing configuration the tail-off stability (fig. 26) is reduced at lower angles of attack (5 degrees) while the tail contribution is maintained effective to higher angles ($17\frac{1}{2}$ degrees, fig. 27). The resulting airplane stability goes from an acceptable level at 5 degrees angle of attack to neutral stability at 20 degrees angle of attack.

LATERAL CONTROL SYSTEM EFFECTIVENESS

Effectiveness of various components of the lateral control system is shown in figure 28 for both clean and landing configurations. The clean aircraft control effectiveness is shown for a typical angle of attack of 5 degrees. Deflection of the inboard spoiler produces a small positive contribution to lateral control. However no rolling moment develops when the mid spoiler is deflected together with the inboard spoiler, indicating a negative contribution due to the mid spoiler. Reversed roll effectiveness of the mid spoiler is confirmed by the increase in total lift when the spoiler is extended, and by pressure data which indicates increased lift. The outboard inverted spoiler/deflector is more effective than the other spoilers and provides roll in the proper direction. The deflectors when used with the mid and inboard spoilers cause increased roll in the wrong direction.

Airplane control effectiveness in the landing configuration is presented at a typical 10 degrees angle of attack. Spoiler effectiveness is satisfactory with the mid and inboard spoilers deflected. The deflectors, which are designed to increase spoiler effectiveness at high speed, have a slight negative effect when used with flaps down. The outboard, inverted spoiler deflector, again intended for high speed use, also has a small negative contribution to rolling moment.

The aileron effectiveness is close to estimated values for both the clean airplane and the landing configuration.

CROSSWIND LANDING CAPABILITY

Crosswind landing capability of the present configuration at a gross weight of 204,117 kg (450,000 pounds) is illustrated in figure 29. At a typical landing speed of 72 m/sec (140 knots) the crosswind component is limited to 15.4 m/sec (30 knots) by maximum roll control. A more conservative limitation of 75 percent of maximum roll control would still allow over 10.8 m/sec (21 knots) of crosswind component.

CONCLUSIONS

Based on the results obtained from the test program the following conclusions are drawn.

- A full-span leading-edge device is required to maximize performance
- 80-percent leading-edge suction is obtained during climb-out after takeoff
- to maximize leading-edge suction with increasing C_L requires increasing leading-edge flap deflection.
- spoilers are preferred over spoiler/deflectors at low-speeds
- pitching moments are nonlinear with a mild pitch-up at 6-degrees angle of attack and are not significantly changed with leading-edge flap deflection

- pitch-up is controllable with horizontal tail
- the vertical tail maintains effectiveness up to highest angle of attack tested (21 degrees)
- tail-on directional stability deteriorates at high angles of attack
- lateral control appears to be adequate for landing at 72 m/sec (140 knots) in a 15.4 m/sec (30 knot) crosswind.

In addition the following low-speed testing requirements for technology readiness are recommended:

- validate drag-due-to-lift characteristics with a high Reynolds number test
- establish that fuselage strakes can improve directional stability
- evaluate suitability of leading-edge slats instead of leading-edge flaps
- evaluate effect on low-speed characteristics of latest configuration changes developed by MDC (increased outer panel sweep)

REFERENCES

1. Radkey, R.L., Welge, H.R., and Felix, J.E.: Aerodynamic Characteristics of a Mach 2.2 Advanced Supersonic Cruise Aircraft Configuration at Mach Numbers from 0.5 to 2.4. NASA CR-145094, 1977.
2. Coe, P.L. and Graham, A.B.: Results of Recent NASA Research on Low-Speed Aerodynamic Characteristics of Supersonic Cruise Aircraft. Proceedings of the SCAR Conference, CP-001, 1977.
3. Shivers, J.P., McLeneore, H.C., and Coe, P.L.: Low-Speed Wind-Tunnel Investigation of a Large-Scale Advanced Arrow Wing Supersonic Transport Configuration With Engines Mounted Above the Wing for Upper-Surface Blowing. NASA TN D-8350, 1976.
4. Friedman, D.M.: A Three-Dimensional Lifting Potential Flow Program. McDonnell Douglas Report MDC J6182, 1974.
5. Coe, P.L. and Weston, R.P.: Effects of Wing Leading-Edge Deflection on the Low-Speed Aerodynamic Characteristics of a Low-Aspect-Ratio Highly Swept Arrow-Wing Configuration. NASA TM 78787, 1978.
6. Coe, P.L., Huffman, J.K.: Influence of Optimized Leading-Edge Deflection and Geometric Anhedron on the Low Speed Aerodynamic Characteristics of a Low-Aspect-Ratio Highly Swept Arrow-Wing Configuration. NASA TM 80083, 1979.

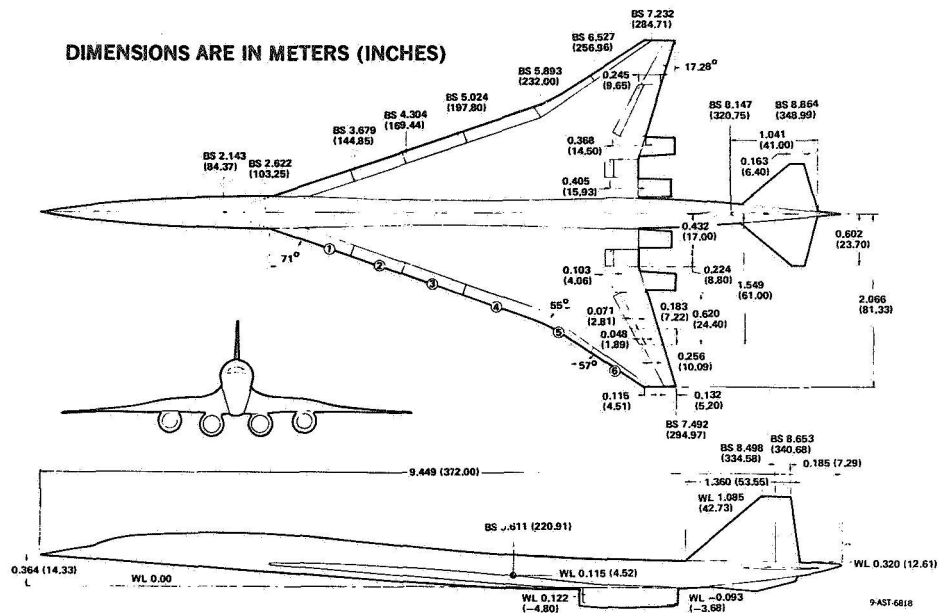


Figure 1.- Three-view drawing of 1/10-scale model.

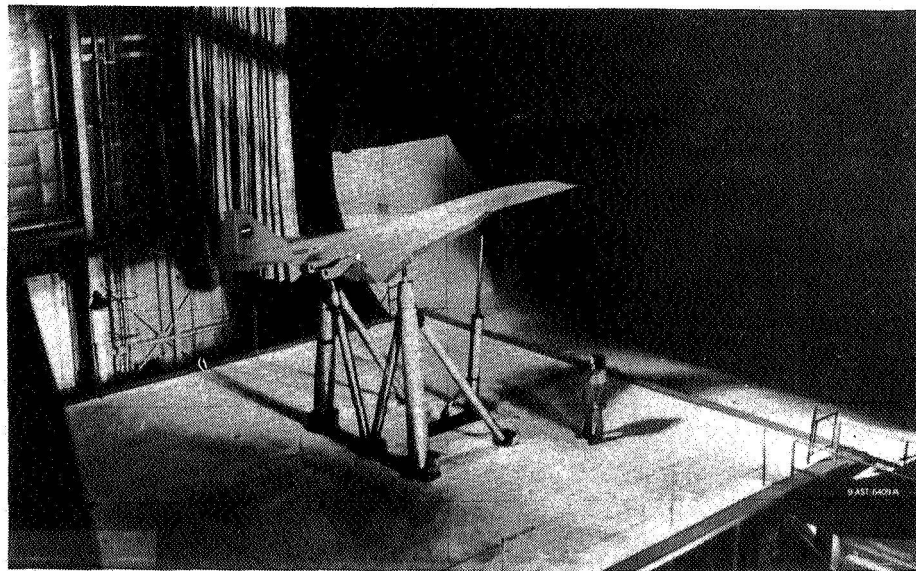


Figure 2.- 1/10-scale low-speed model in Langley 30- by 60-ft tunnel.

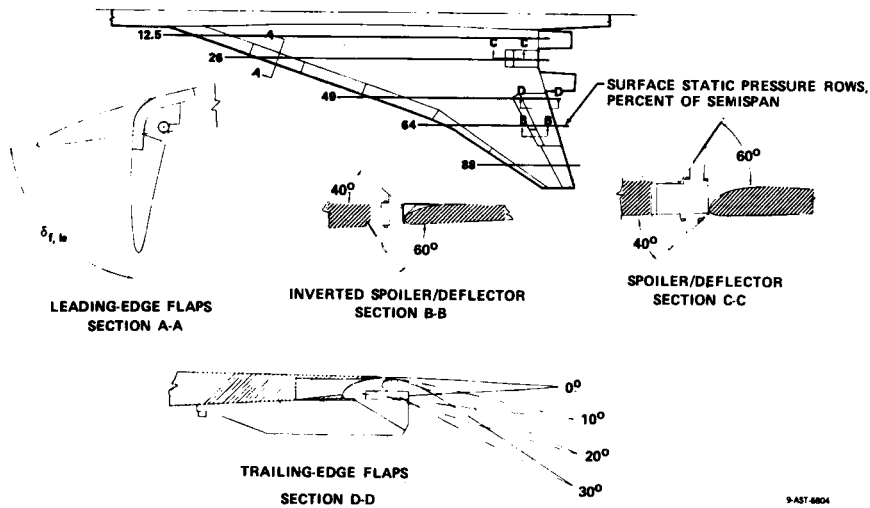


Figure 3.- Schematic drawings of leading- and trailing-edge flaps, spoiler/deflector, and inverted spoiler/deflector.

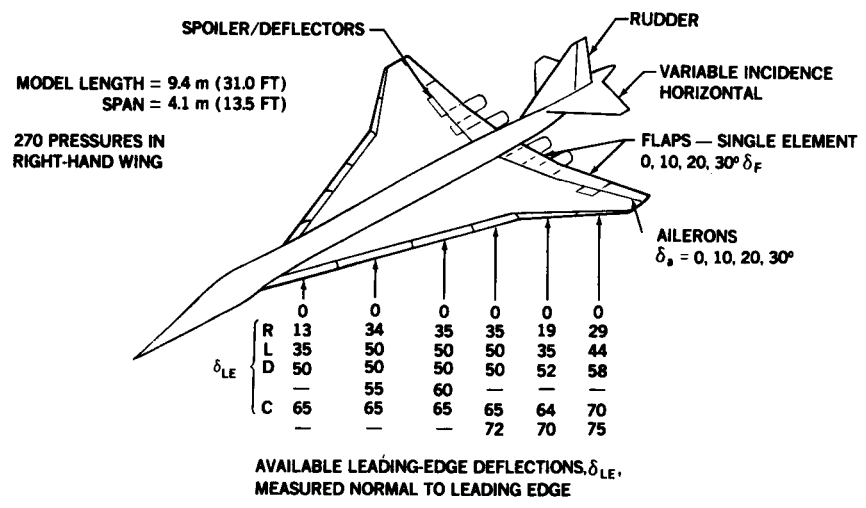


Figure 4.- Variable geometry features of 1/10-scale low-speed model.

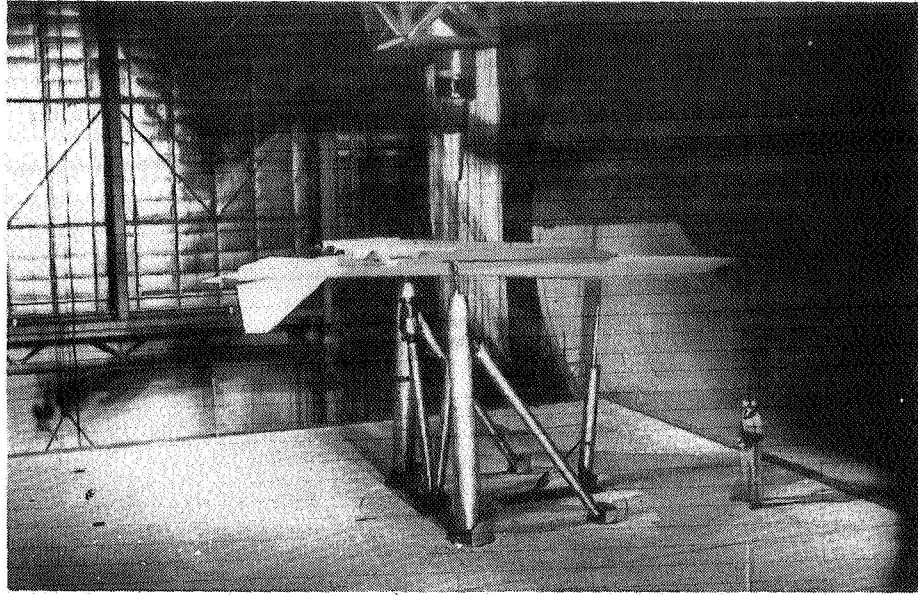


Figure 5.- Inverted model installation with dummy strut.

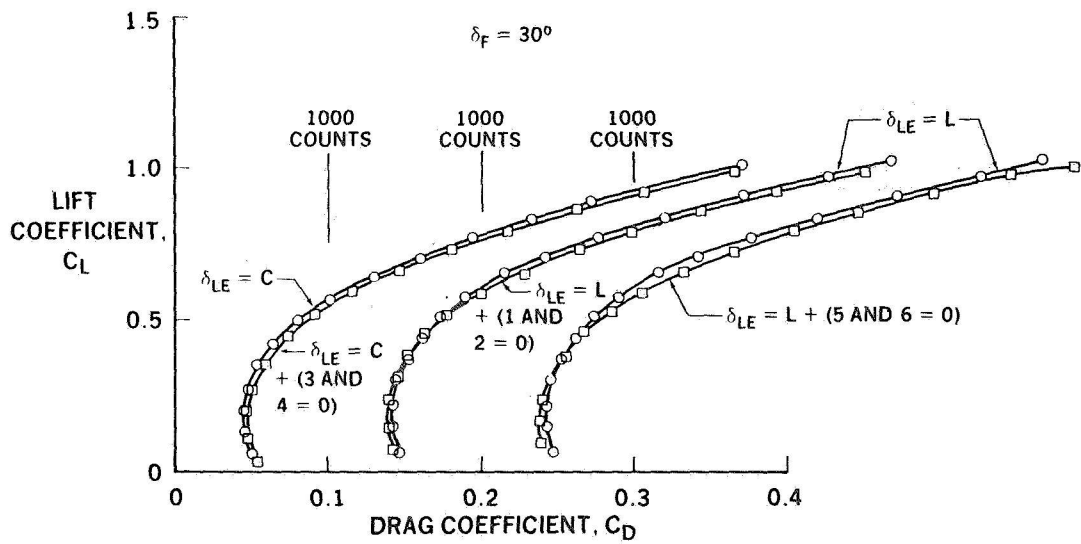


Figure 6.- Drag comparison of full and partial leading edge deflections.

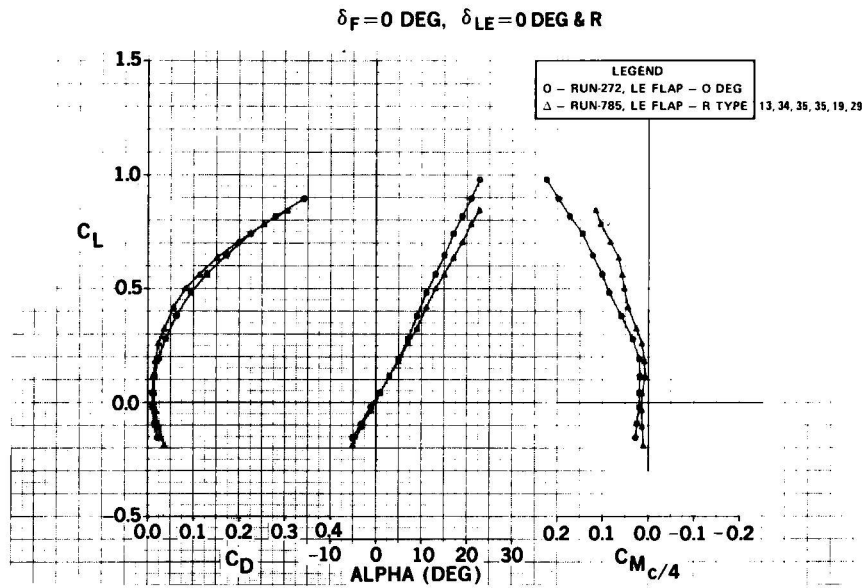


Figure 7.- Leading edge flap effectiveness.

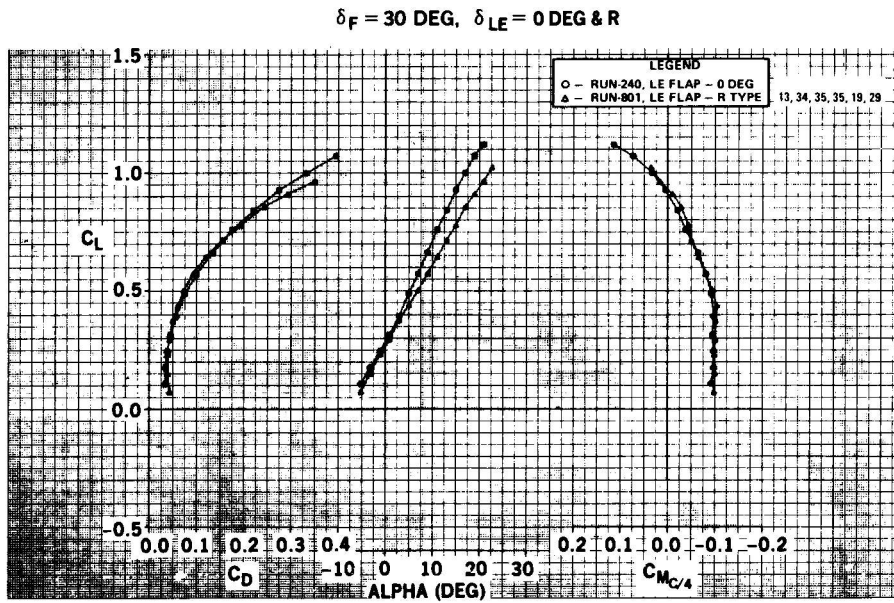


Figure 8.- Leading edge flap effectiveness.

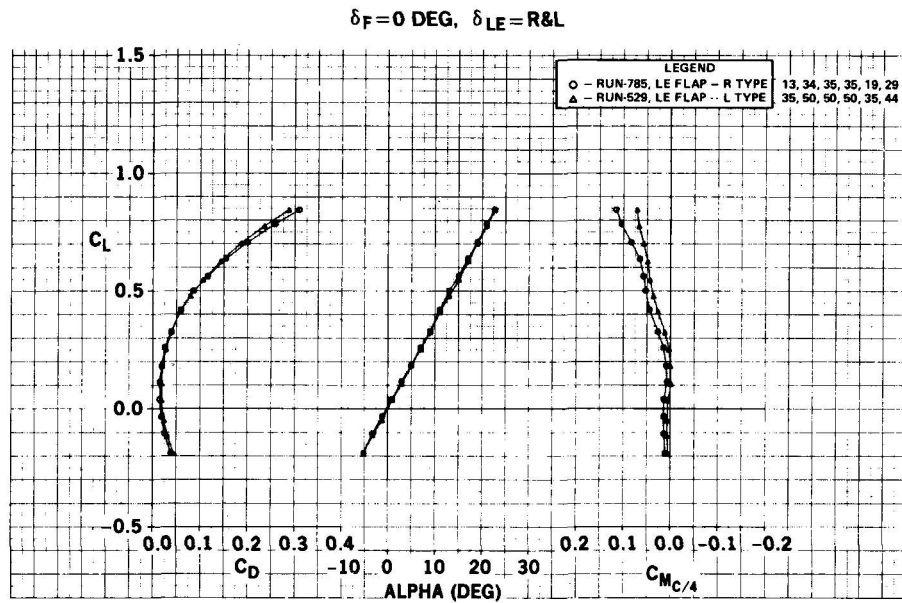


Figure 9.- Leading edge flap effectiveness.

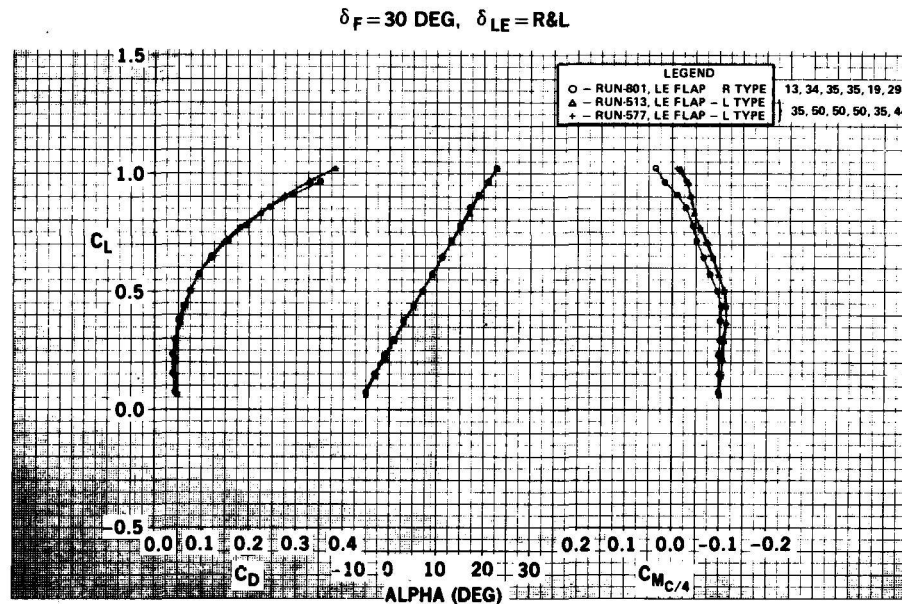


Figure 10.- Leading edge flap effectiveness.

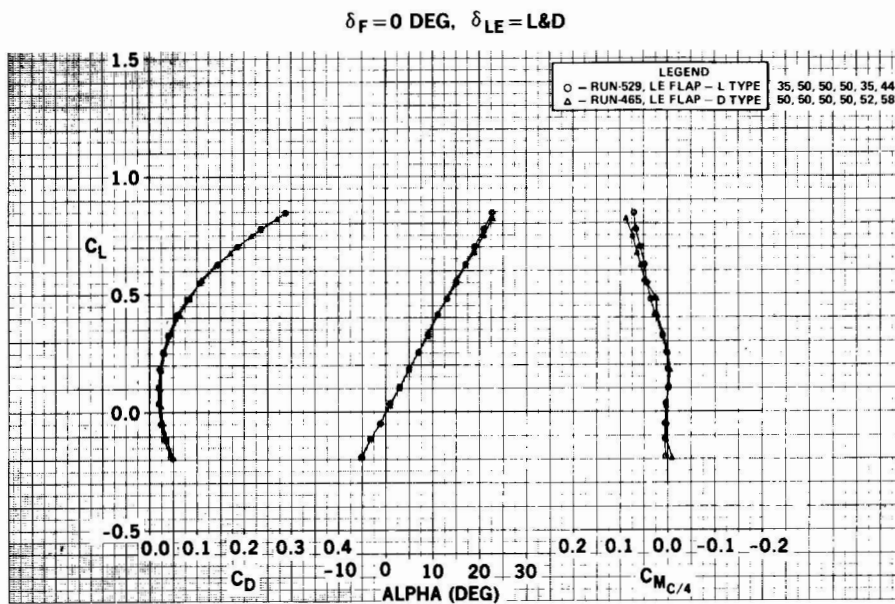


Figure 11.- Leading edge flap effectiveness.

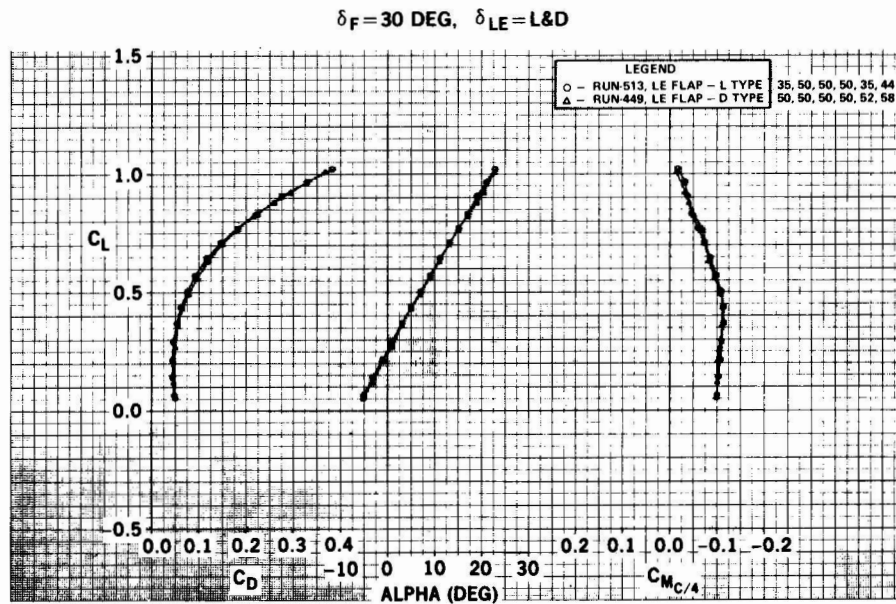


Figure 12.- Leading edge flap effectiveness.

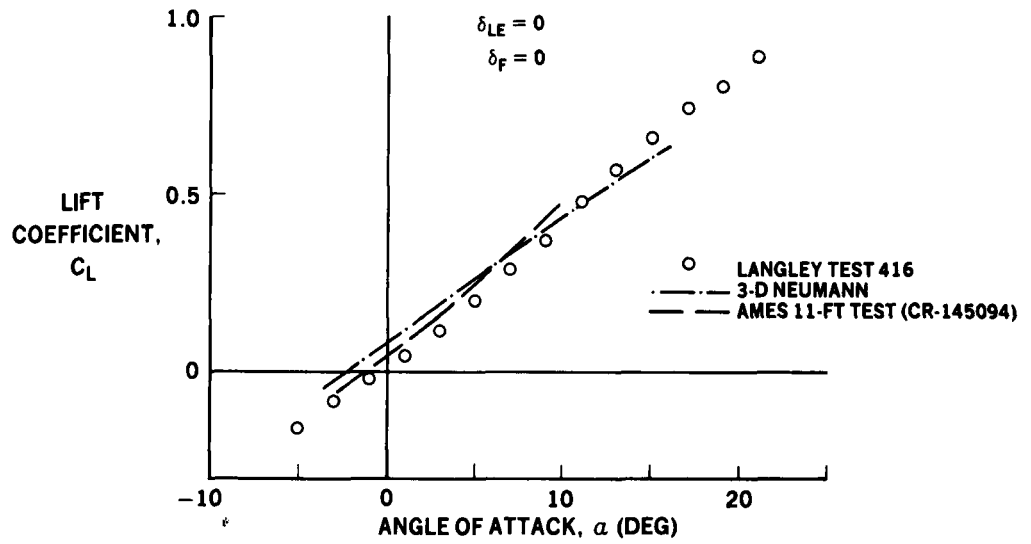


Figure 13.- Comparison of clean wing lift characteristics.

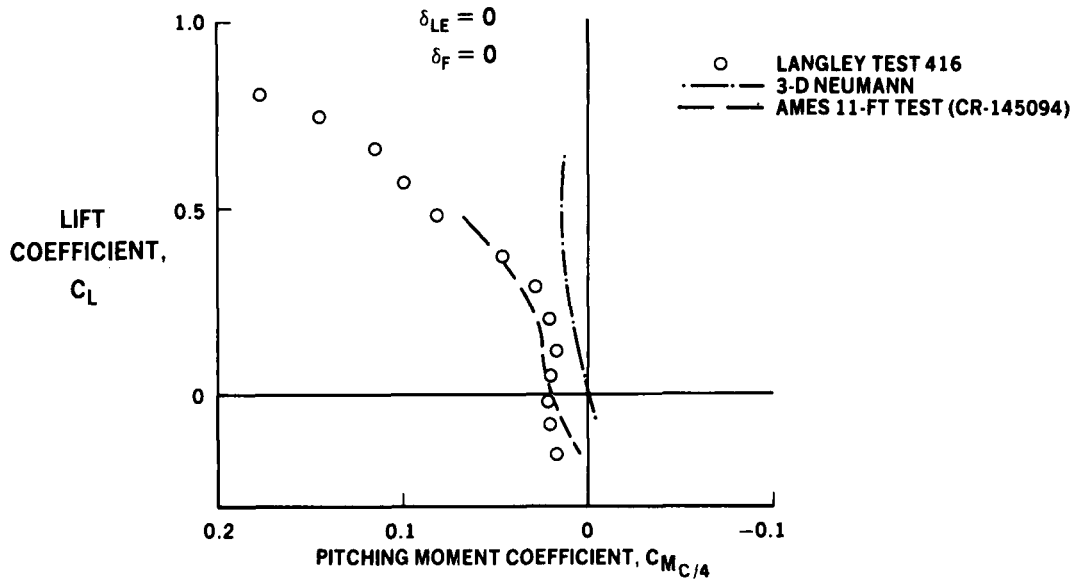


Figure 14.- Comparison of clean wing pitching moment characteristics.

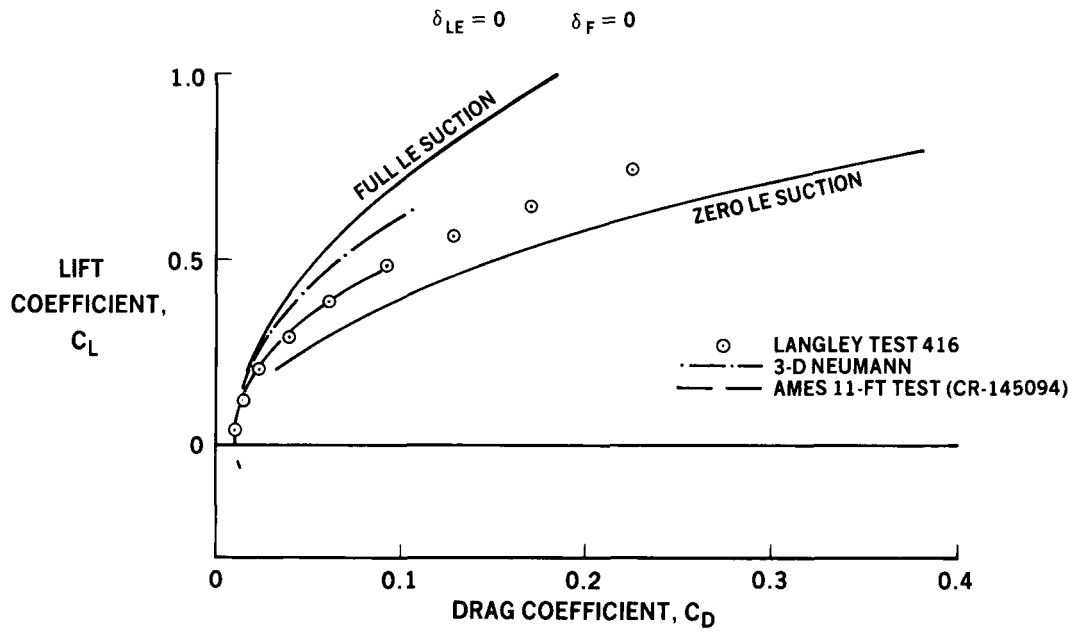


Figure 15.- Comparison of clean wing drag polars.

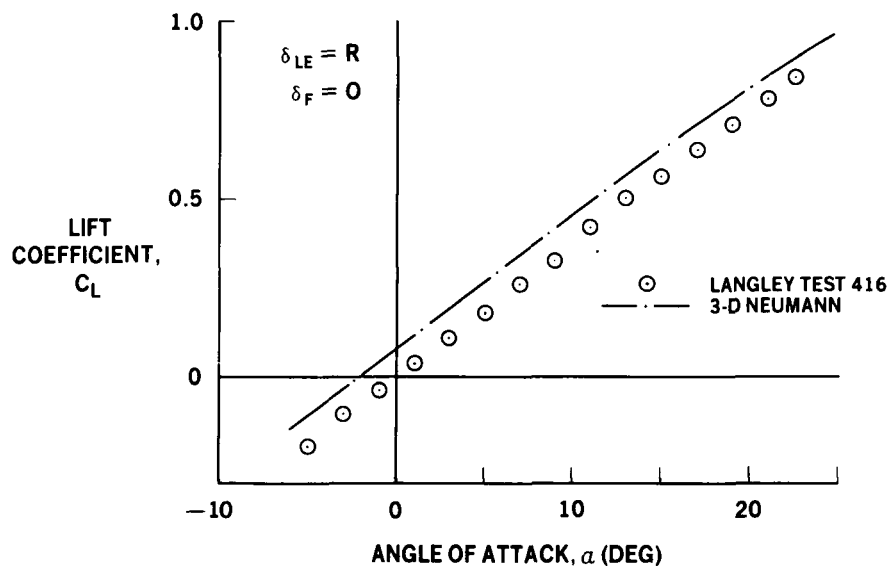


Figure 16.- Lift characteristics with leading edge deflected.

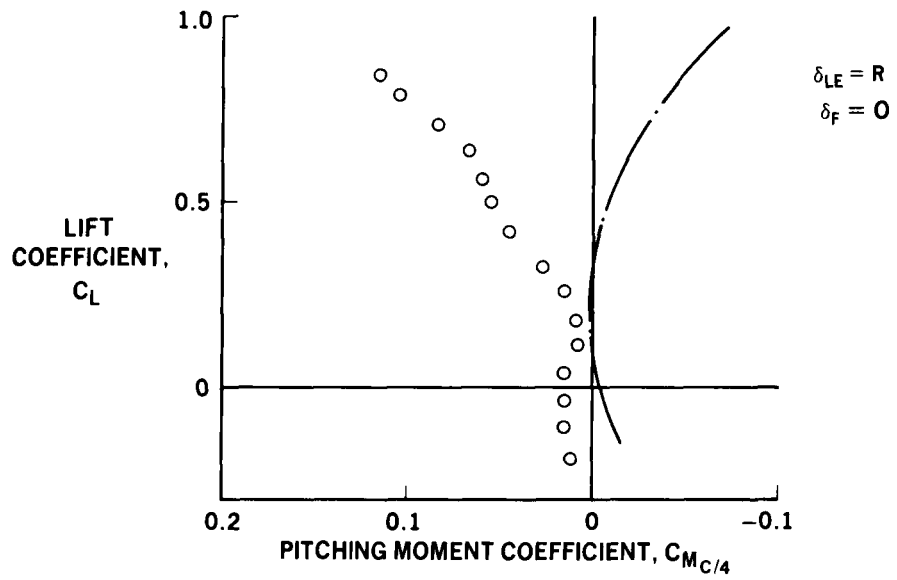


Figure 17.- Pitching moments with leading edge deflected.

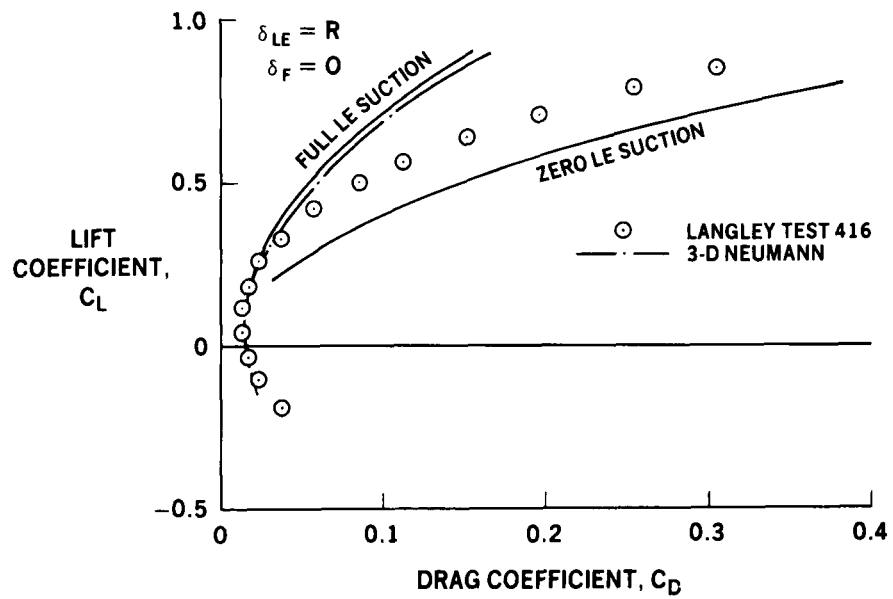


Figure 18.- Drag polars with leading edge deflected.

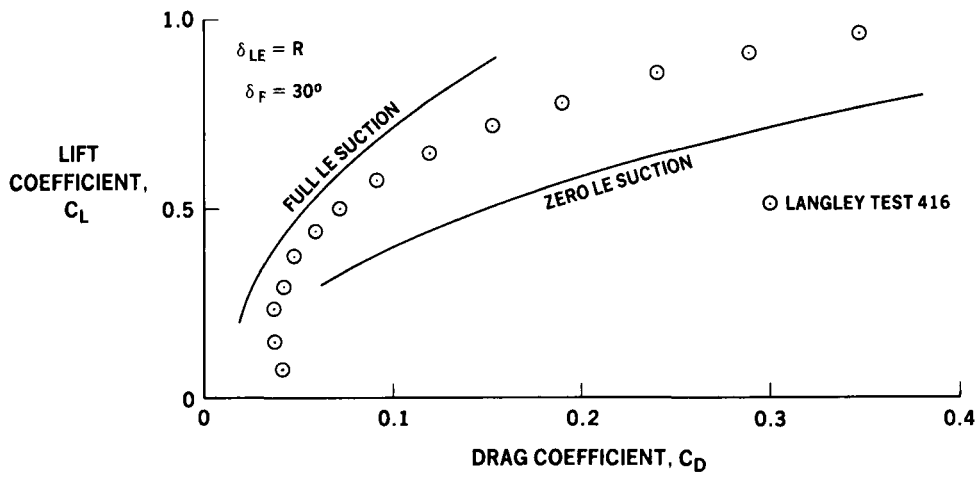


Figure 19.- Drag polar with leading and trailing edge deflected.

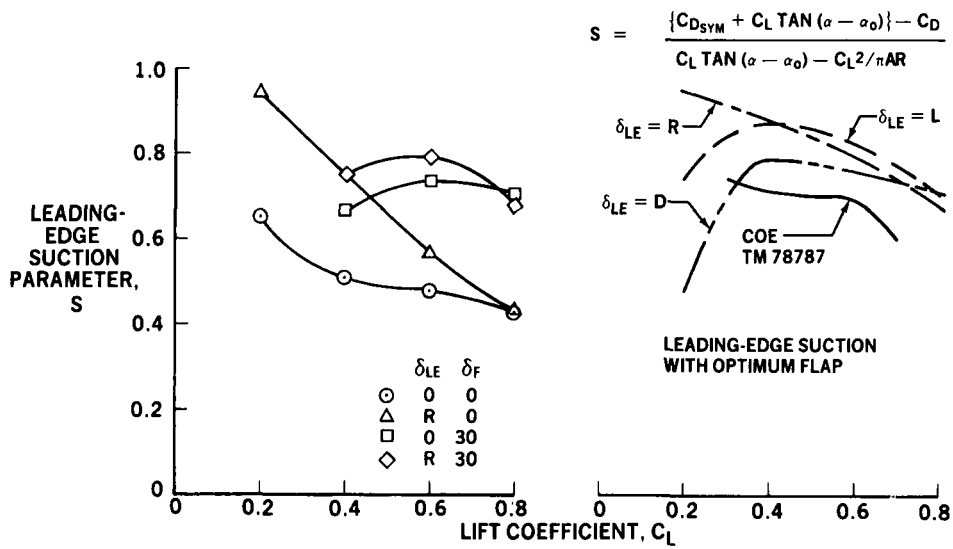


Figure 20.- Leading-edge suction characteristics.

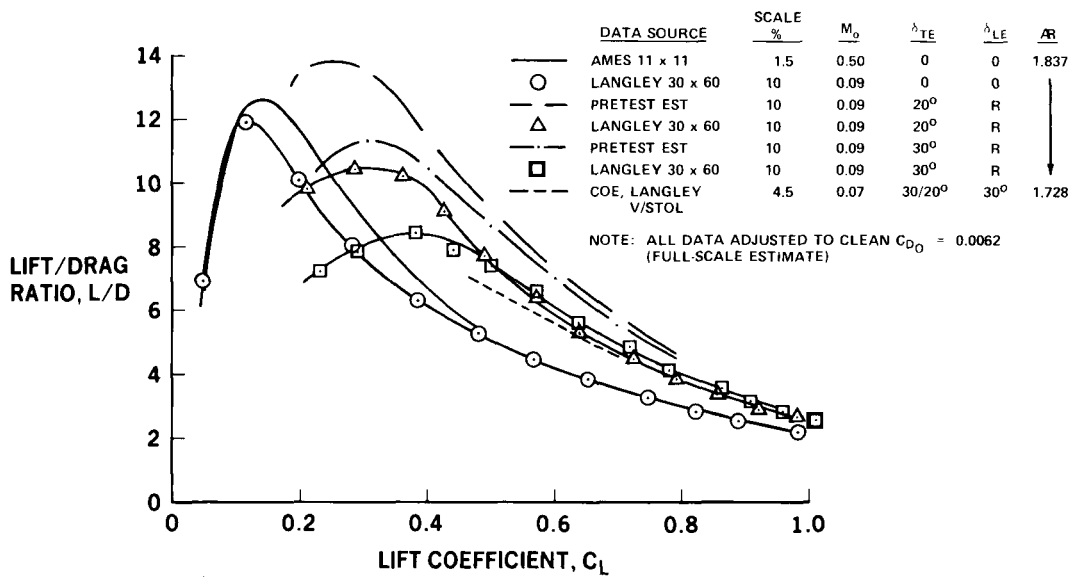


Figure 21.- Low-speed L/D summary, untrimmed.

UPPER SURFACE ONLY

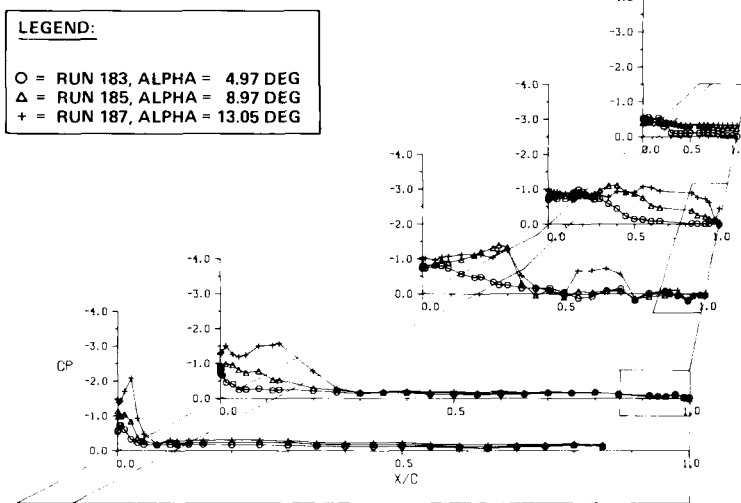


Figure 22.- Effect of angle of attack on clean wing pressure distribution.

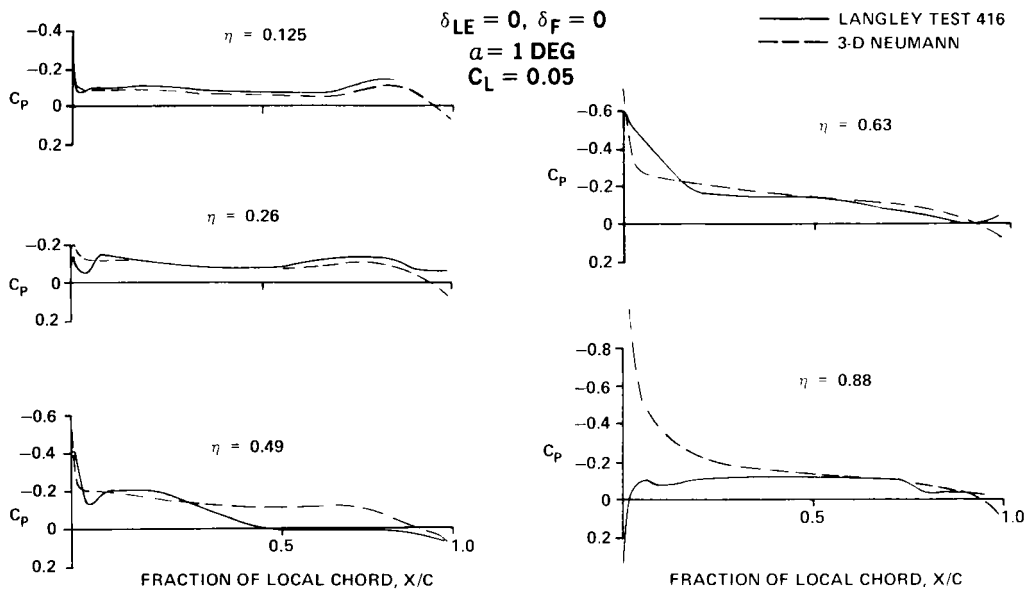


Figure 23.- Comparison of experimental upper surface pressures with theory.

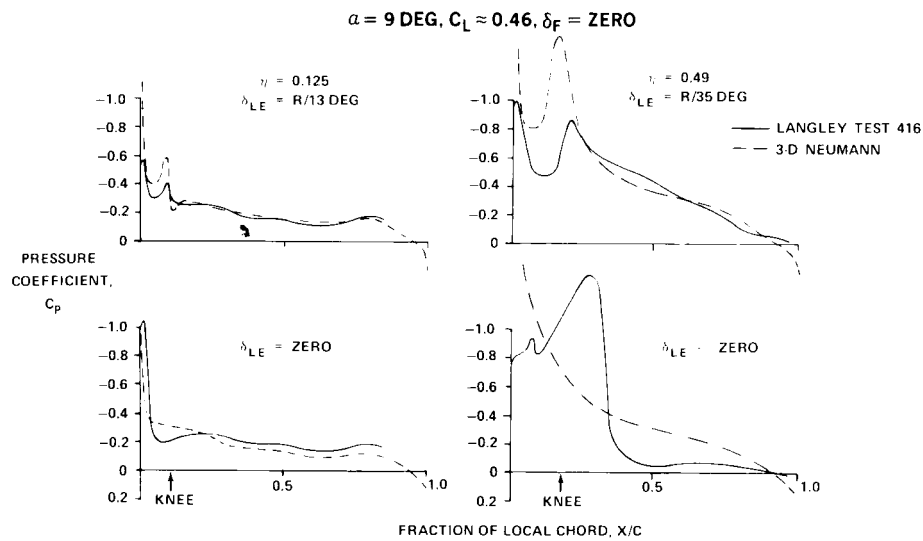


Figure 24.- Comparison of Neumann pressure distributions with data, with and without leading edge deflected.

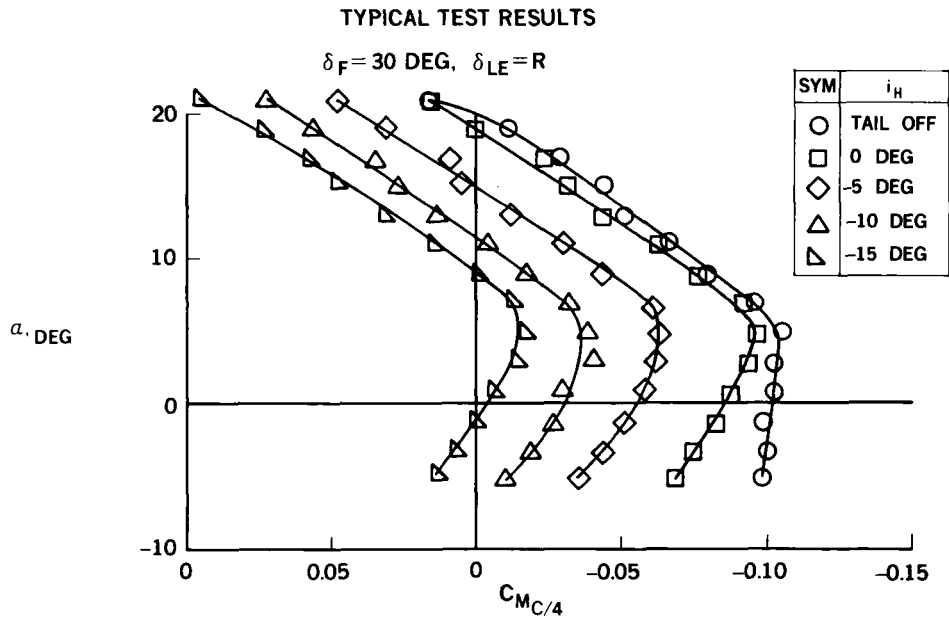


Figure 25.- Horizontal tail effectiveness.

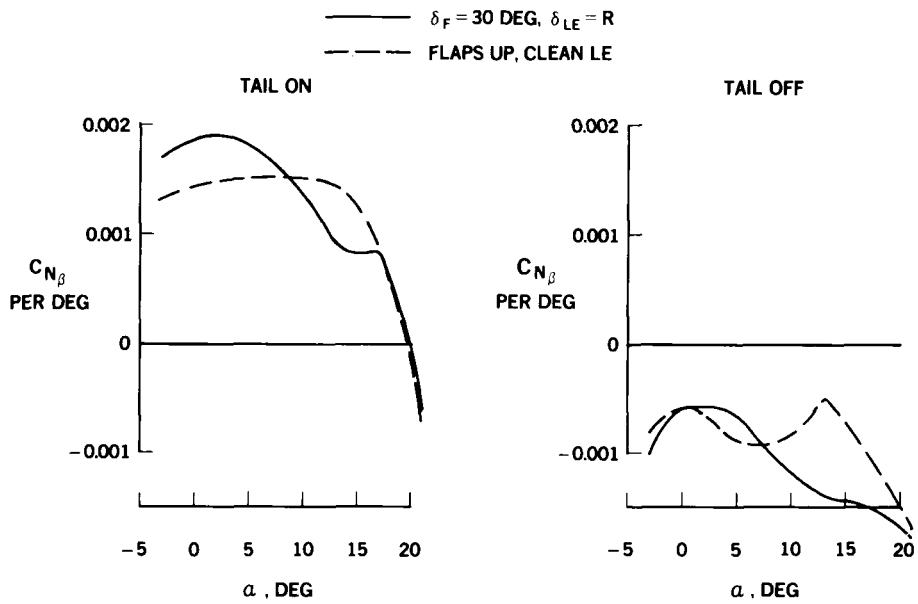


Figure 26.- Directional stability.

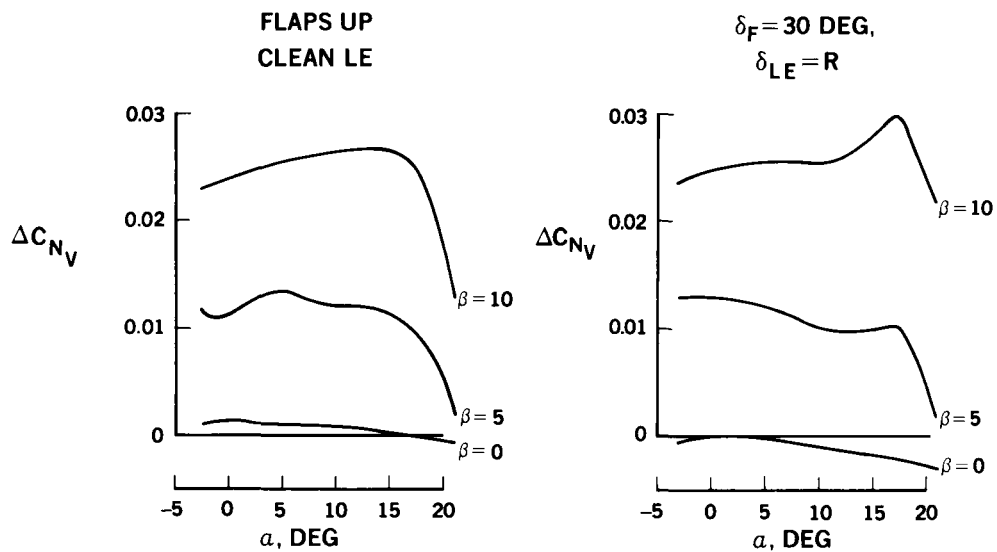


Figure 27.- Vertical tail effectiveness.

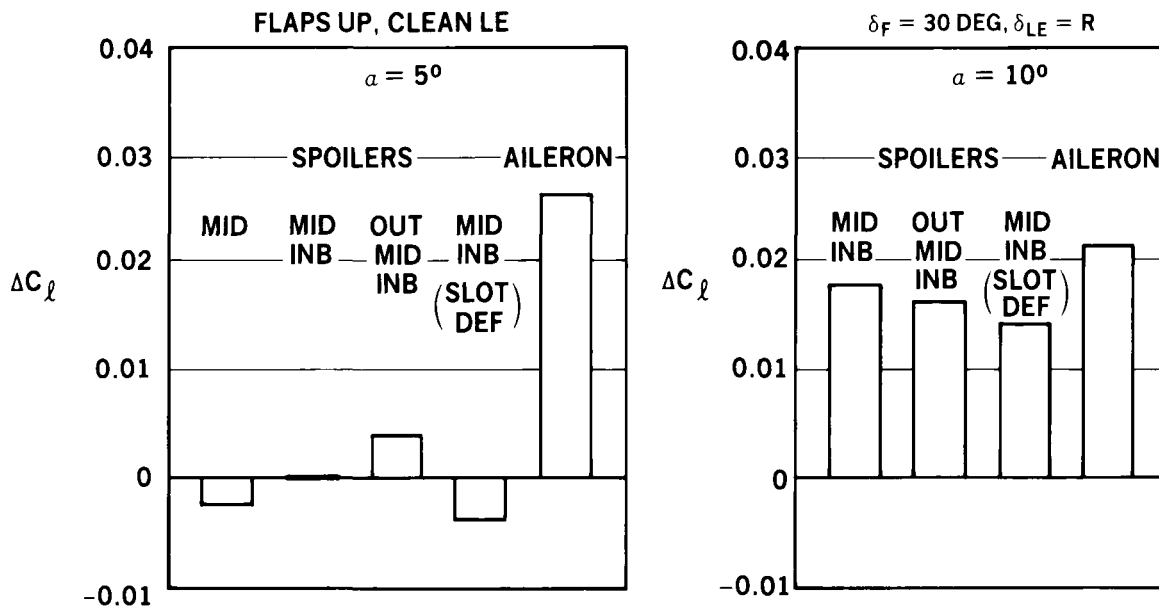


Figure 28.- Lateral control system effectiveness.

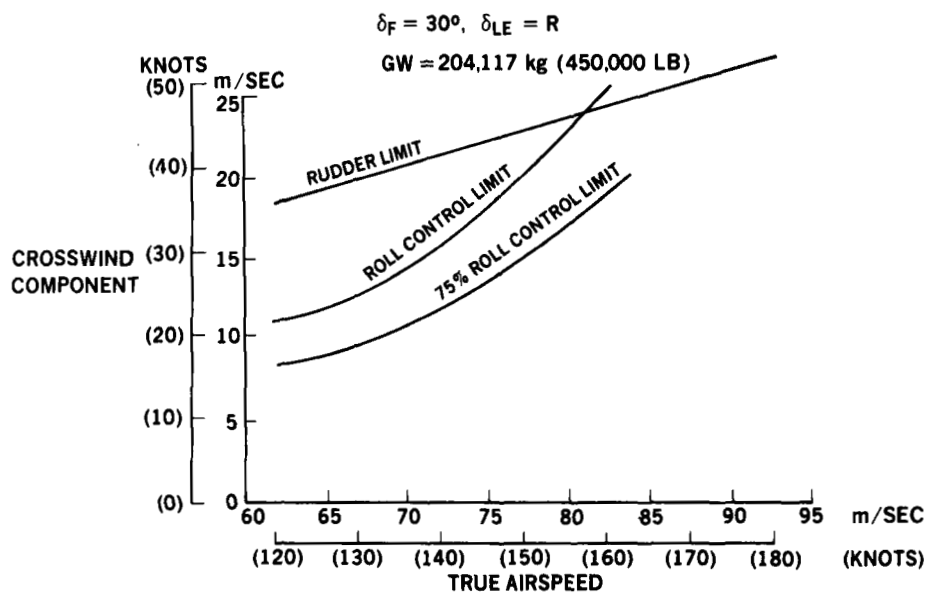


Figure 29.- Estimated cross-wind landing capability.